Chinese Chemical Letters 35 (2024) 109108

Contents lists available at ScienceDirect

Chinese Chemical Letters

journal homepage: www.elsevier.com/locate/cclet

The compatibly large nonlinear optical effect and high laser-induced damage threshold in a thiophosphate $CsInP_2S_7$ constructed with $[P_2S_7]^{4-}$ and $[InS_6]^{9-}$

Mengjia Luo [a,1], Xiaohui Li [d,1], Xingxing Jiang [c,*], Zheshuai Lin [c], Zhengyang Zhou [b,*]

[a] Nanchang Key Laboratory of Photoelectric Conversion and Energy Storage Materials, Nanchang Institute of Technology, Nanchang 330099, China
[b] Shanghai Institute of Ceramics, Chinese Academy of Sciences, Shanghai 200050, China
[c] Functional Crystals Lab, Technical Institute of Physics and Chemistry, Chinese Academy of Sciences, Beijing 100190, China
[d] Institute of Experimental Physics, Free University Berlin, Berlin D-14195, Germany

ARTICLE INFO

Article history:
Received 11 July 2023
Revised 20 August 2023
Accepted 14 September 2023
Available online 16 September 2023

Keywords:
Infrared nonlinear optics materials
A novel thiophosphate
Structure design
Structure-activity relationship
High laser-induced damage threshold

ABSTRACT

It is challenging to cooperatively improve the nonlinear optical (NLO) efficiency and the laser-induced damage threshold (LIDT). This work reports a novel IR NLO materials $CsInP_2S_7$ (CIPS) designed by combination the strategies of alkali metals substitution and microscopic NLO units PS_4 introduction based on $AgGaS_2$. CIPS was composed of strongly distorted $[InS_6]^{9-}$ octahedra and $[P_2S_7]^{4-}$ dimers constructed by corner-sharing $[PS_4]^{3-}$, which increase the NLO efficiency and decrease thermal expansion anisotropy simultaneously. Compared with $AgGaS_2$, CIPS exhibited strong phase matchable NLO response *ca.* $1.1 \times$ AGS@2.1 μm, high LIDT *ca.* $20.8 \times AgGaS_2$, and IR transparency up to 15.3 μm. Structural analysis and theoretical investigation confirmed that large SHG effect and ultrahigh LIDT of CIPS originated from the synergistic contribution of $[InS_6]^{9-}$ octahedra and $[P_2S_7]^{4-}$ dimers. These results indicate that CIPS is a promising NLO candidate in the mid-IR region, and this study provides a new approach for developing potential NLO-LIDT compatible materials.

To release medical diagnostics, atmospheric detection, laser guidance and laser telecommunications, coherent tunable lasers in the mid-IR region (2–20 μm) are very necessary [1,2]. Infrared nonlinear optical (IR NLO) materials can convert near IR light to mid-IR band *via* frequency down-conversion, which play important roles in solid state laser technology [3]. However, the commercially available middle-IR (MIR) NLO crystals are relatively rare. Notably, $AgGaS_2$ (AGS), $AgGaSe_2$ and $ZnGeP_2$, featuring large NLO coefficients, are the only available commercial IR NLO materials [4–6]. Nonetheless, they still suffer from intrinsic defects such as harmful two-photon absorption (TPA) of $ZnGeP_2$ and low laser-induced damage thresholds (LIDTs) of AGS and $AgGaSe_2$, which severely limit their high-power laser applications. As a result, they cannot achieve a good balance between large second-harmonic generation (SHG) and high LIDT. Therefore, systematic explorations of new IR NLO materials to realize NLO-LIDT compatible have become a research hot-spot.

Alkali-metal possess high electro-positivity and large ionic radius. When alkali-metal was introduced into a compound, the band gap and local structure distortion of this compound will increase [7,8]. Therefore, alkali-metal atoms substitution is a common regulation strategy for IR NLO materials to increase properties, such as $Rb_{10}Zn_4Sn_4S_{17}$ (NLO response: $0.7 \times$ AGS; LIDT: $5 \times$ AGS) [9]. In addition, introduction of NLO active units or complex coordinated functional groups is a good strategy to discover new materials whose NLO efficiencies and LIDTs are balanced [10–19]. Among numerous active units, PS_4 has short P-S bond length and small volume, and PS_4 units can form other active NLO units such as edge-sharing P_2S_6 [20]. Moreover, thiophosphates possess wide IR transparency ranges, such as $Hg_3P_2S_8$ (NLO response: $4.2 \times$ AGS@2.09 μm, optical transmitting range: 0.45–16.7 μm), $Eu_2P_2S_6$ ($0.9 \times$ AGS@2.1 μm, 0.49–15.4 μm), $AgGa_2PS_6$ ($1 \times$ AGS@2.1 μm, 0.60–16.7 μm), thus attracting extensive attention [13,21,22].

In this work, a new compound $CsInP_2S_7$ (CIPS) was obtained by combination the strategies of alkali metals substitution and microscopic NLO units PS_4 introduction based on $AgGaS_2$. Ag^+ was replaced by Cs^+ cation and PS_4 unit was introduced to replace S site. In order to maintain structural stability, In^{3+} cation with flex-

* Corresponding authors.
E-mail addresses: xxjiang@mail.ipc.ac.cn (X. Jiang), zhouzhengyang@mail.sic.ac.cn (Z. Zhou).
[1] These authors contributed equally to this work.

https://doi.org/10.1016/j.cclet.2023.109108
1001-8417/

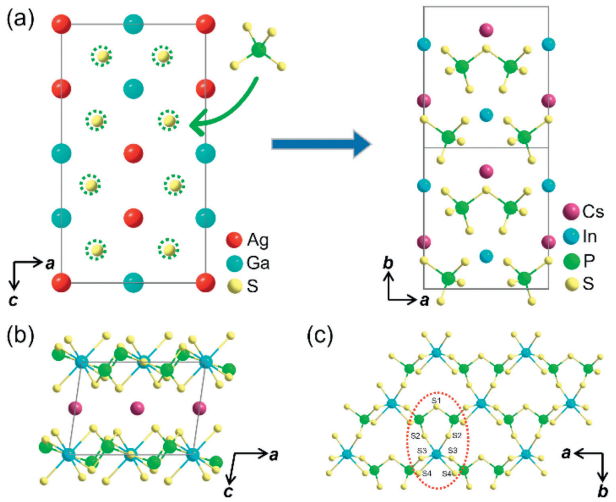

Fig. 1. (a) Schematic diagram of the structural evolution from $AgGaS_2$ to $CsInP_2S_7$. (b) 2D $[InP_2S_7]^-$ anionic framework of CIPS, Cs^+ cations are filled in the interlayer space. (c) $[InP_2S_{11}]^{9-}$ ring in red circle and $[P_2S_7]^-_\infty$ layer in the ab plane.

ible coordination number (4, 6, and 8) was introduced to coordinate with S atoms of $[PS_4]^{3-}$ (Fig. 1a). The CIPS exhibits a wide optical transmittance in the range of 0.414–15.3 μm, strong phase-matchable NLO response *ca.* 1.1 × AGS@2.1 μm, and high LIDT *ca.* 20.8 × AGS. Through the structural analysis and first-principles calculations, the origin of optical properties from cooperation of the $[InS_6]^{9-}$ and $[P_2S_7]^{4-}$ groups was revealed. It was proposed that alkali metals substitution combined with microscopic NLO units introduction based on known mother materials could be a new method for materials design, which could maintain the original structural framework with large effects and modulate the LIDT performance.

Light yellow plate-like crystals of CIPS were obtained through solid-state reaction with mixture containing In, P_2S_5, S, and CsCl at 1223 K (see detailed description in Supporting information). The powder X-ray diffraction (PXRD) pattern matches well with the calculated results based on single-crystal XRD analysis (Fig. S1 in Supporting information). The corresponding crystallographic data are summarized in Tables S1–S3 (Supporting information). Energy dispersive spectroscopy (EDS) analysis confirms the presence of Cs, In, P, and S elements with the approximate molar ratio of 1:1:2.02:6.97 (Fig. S2 in Supporting information), which is consistent with the single-crystal XRD analysis.

CIPS crystallizes in the Non centrosymmetric monoclinic space group *C*2 (No. 5) and features a 2D $[InP_2S_7]^-$ layer with Cs^+ cations filled in the interlayer space (Fig. 1b). The $[InS_6]^{9-}$ octahedra and the $[P_2S_7]^{4-}$ dimers share S2 atoms to form $[InP_2S_{11}]^{9-}$ rings (Fig. 1c). The $[InP_2S_{11}]^{9-}$ rings connected to another one *via* edge-sharing and then form the 2D $[InP_2S_7]^-$ anionic framework. To maintain charge balance, Cs^+ cations get filled in the interlayer space. The In−S bond lengths in the $[InS_6]^{9-}$ polyhedra range from 2.587(3) Å to 2.686(3) Å (Fig. S3a in Supporting information), which are in accordance with $CuInP_2S_6$ [23]. The P-S bond lengths in $[P_2S_7]^{4-}$ dimers, ranging from 2.007(5) Å to 2.142(3) Å (Fig. S3b in Supporting information), are close to those in $SnPS_3$, $Zn_3P_2S_8$ [24,25]. The distances between Cs and S in $[CsS_{10}]^{19-}$ polyhedra range from 3.533(3) Å to 4.062(3) Å (Fig. S3c in Supporting information), comparable to those in $CsVP_2S_7$ [26].

Details of the structure evolution from AGS to CIPS were shown in Fig. S4 (Supporting information). The red-line circled part (A) and blue-line circled part (B) in the structure of CIPS correspond to an infinitely extended $[InP_2]$ layer and $[CsInP_3]$ layer (Figs. S4b and c), which is highly similar with the red-line circled part (A') and blue-line circled part (B') in the structure of AGS, respectively (Figs. S4e and f). Compared with the two isolated four-connected S atoms in AGS, the PS_4 units in CIPS are linked to form $[P_2S_7]^{4-}$ dimers due to the introduction of the strongly distorted $[InS_6]^{9-}$ octahedron, which makes CIPS with alkali metal inherit the effective framework from AGS, and still brings about the effective superposition of microscopic second-order nonlinear susceptibility.

Table 1
Thermal expansion coefficients α_L ($\times 10^{-5}$ K^{-1}) of the *a*, *b*, and *c* axis, and the thermal expansion anisotropy.

Coefficient	CIPS	AGS
$\alpha_L(a)$	0.66	3.08
$\alpha_L(b)$	1.44	3.08
$\alpha_L(c)$	0.39	−9.16
TEA[a]	0.84	1.60

[a] $TEA = \frac{|\alpha_a - \alpha_b| + |\alpha_a - \alpha_c| + |\alpha_b - \alpha_c|}{|\alpha_a| + |\alpha_b| + |\alpha_c|}$ [38].

The Rietveld refinement against the PXRD patterns of the samples used for SHG response evaluation on dry powder reveals that almost no impurity is involved, and this confirms that the measured result is intrinsic property of CIPS (Fig. 2a). According to the TG-DTA result, CIPS starts to lose weight significantly at around 192 °C, corresponding to the decomposition (Fig. S5 in Supporting information). CIPS exhibits typical phase-matching behavior, *i.e.*, a tendency to increase gradually to platform of SHG intensities with the increase in particle size (Fig. 2b). The SHG response of pure polycrystalline dry CIPS powder (Fig. 2c) was measured using a Q-switch laser (2.1 μm), and AGS was used as the Ref. [27]. Moreover, the SHG efficiency of CIPS is ~1.1 × AGS at the largest particle size range of 200–250 μm. Such SHG responses are moderate compared with other promising IR-NLO chalcogenides, including $LiZnPS_4$ (0.8 × AGS), $Sn_7Br_{10}S_2$ (1.5 × AGS), and $LaBS_3$ (1.2 × AGS) [28–30]. Hitherto, some thiophosphates (Table S4 in Supporting information) with good NLO performances were studied. However, most of them are formed with $[PS_4]^{3-}$ units and $[P_2S_6]^{4-}$ dimers, except for $Rb_2Ga_2P_2S_9$ (0.1 × AGS) with $[P_2S_7]^{4-}$ dimers [31].

The experimental E_g of CIPS was deduced from the UV–vis–NIR transmittance spectrum to be 3.0 eV (Fig. 2d), larger than that of the commercial AGS (2.56 eV) and enough to get away from the drawback of TPA (2.33 eV, 532 nm). The IR cutoff edge of CIPS was verified by IR transmittance spectra, and it was measured to be about 15.3 μm, which covers two atmospheric windows of 3–5 and 8–12 μm. Several absorption peaks are present at 8–11 μm in the IR transmittance spectra, which is possibly caused by multi-phonon absorption and the similar phenomenon is also found in $Hg_3P_2S_8$ and $CuZnPS_4$. Therefore, CIPS shows a transparency of 0.414–15.3 μm, superior to that of the commercial mid-IR NLO crystals of AGS (0.48–11.4 μm) and similar to the other reported thiophosphates, such as $CuHgPS_4$ (0.54–16.7 μm) and $CuZnPS_4$ (0.43–16.5 μm) [21,32,33].

Corresponding to the larger band gap, the LIDT is always higher. Through the evaluation of LIDT, CIPS shows 20.8 times higher LIDT than AGS (Table S5 in Supporting information), which is consistent with the general observation that the E_g and LIDT are somewhat positively correlated. Apart from the influence of band gap, materials with a smaller thermal expansion anisotropy (TEA) could suffer greater thermal shock due to the temperature increase under laser irradiation and exhibits higher LIDT [34]. Fig. 3a shows the unit-cell variations in parameters of CIPS as a function of temperature by *in situ* PXRD characterization in the range of 293–473 K. Based on these data, the TEA of CIPS (0.84) is smaller than that of AGS (1.60) (Table 1). According to the above-mentioned structural analysis, the two S sites in AGS are isolated without interaction, so that AGS exhibits negative thermal expansion (NTE) behaviors along *c* direction. However, in CIPS, the S sites are replaced with two $[PS_4]^{3-}$ units linked with S to form $[P_2S_7]^{4-}$ dimers and

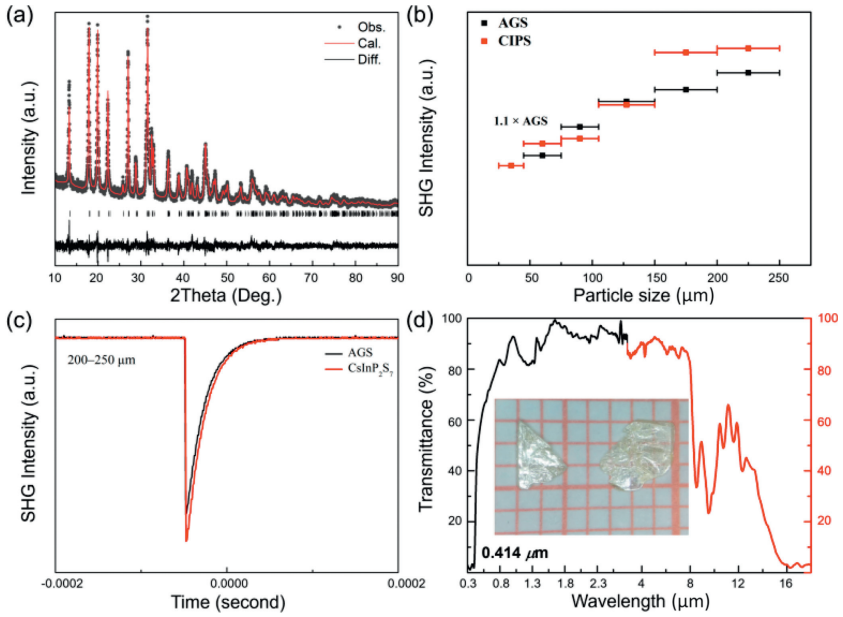

Fig. 2. (a) Rietveld refinement for the powder X-ray diffraction pattern of CIPS. (b) SHG signals of CIPS and AGS for particle sizes of 200–250 μm. (c) The size-dependent SHG responses of CIPS and AGS when irradiated by a 2.1 μm laser. (d) UV–vis–NIR diffuse reflectance spectra and FT-IR spectra for CIPS.

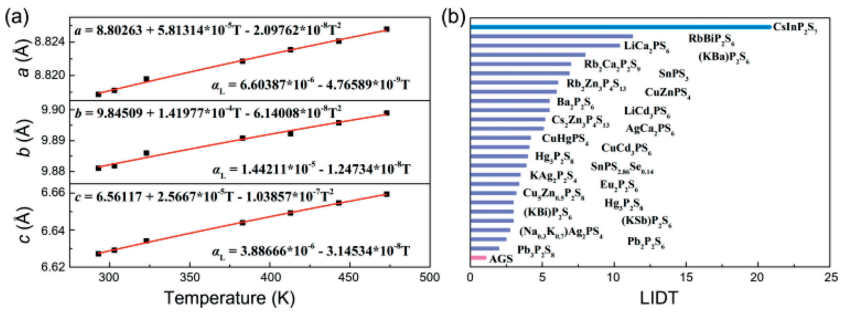

Fig. 3. (a) Comparison of LIDT among NLO thiophosphates. (b) Temperature-dependent lattice parameters of CIPS.

possesses the interaction along *a* direction, which prevents CIPS to have NTE capability and reduces the TEA of CIPS, leading to significant increase in LIDT value. The LIDT of CIPS is better than or comparable with those of the recently reported distinguished IR-NLO chalcogenides, such as $SnI_4{\cdot}(S_8)_2$ (16.4 × AGS), Ga_2Se_3 (16.7 × AGS), and $Na_2Ga_2GeS_6$ (18.1 × AGS) [35–37]. Such an ultrahigh LIDT indicates that CIPS may undergo high-power laser radiation and may offer potential application prospects in the laser frequency conversion system. Overall, comparison among NLO thiophosphates (Fig. 3b) indicates that CIPS is a promising IR NLO candidate.

To better understanding the relationships between structure and property of CIPS, first-principles theoretical calculations, including electronic structure, density of states (DOSs), and optical property were performed. CIPS is an indirect band gap semiconductor with a band gap of 2.01 eV based on theoretical calculation result (Fig. 4a). The simulated value is slightly smaller than that of the measured value (3.0 eV) originating from the intrinsic drawbacks of the PBE functional. Fig. 4b exhibits the total density of state (TDOS) and the partial density of state (PDOS) curves. The upper region of valence bands (VBs) is primarily derived from P 3p, S 3p, and In 4p orbitals, while the bottom part of conduction bands (CBs) mainly consists of P 3s3p, S 3p, and In 4s orbitals. It indicates the existence of strong covalent interactions among In, P, and S atoms. This result reveals that the electronic states close to the Fermi level are mainly contributed by $[InS_6]^{9-}$ and $[P_2S_7]^{4-}$ units. The optical property of a crystal principally arises from the electron transition across the forbidden bands, as a result, the SHG efficiency mainly originates from synergistic interactions between $[InS_6]^{9-}$ and disordered $[P_2S_7]^{4-}$ units.

CIPS crystallizes in the *C*2 space group and exhibits four (χ_{14}, χ_{21}, χ_{22}, and χ_{23}) independent non-zero SHG tensors according to the Kleinman's symmetry rule. The SHG tensors χ_{14}, χ_{21}, χ_{22} and χ_{23} were calculated to be 16.43, 20.19, 16.89, and −4.74 pm/V, respectively, which agree well with the results of SHG measurement. To unveil the main contribution in generating the SHG effect, the SHG-density analysis was conducted. Fig. 4c and Fig. S6 (Supporting information) exhibit that SHG-weighted electronic clouds are mostly localized on $[InS_6]^{9-}$ and $[P_2S_7]^{4-}$ units, while no SHG density occurs around Cs^+ cations. It confirms that the SHG response originates from the $[InS_6]^{9-}$ and $[P_2S_7]^{4-}$ units, matching the conclusion of electronic structure analysis. The birefringence index Δn of CIPS are 0.10@1064 nm and 0.094@2100 nm (Fig. 4d), which meets the requirements of moderate birefringence Δn (~0.03–0.10) [39]. Noteworthy, this moderate Δn could achieve its phase matching capacity in the mid-IR region, which is consistent with the experimental results.

Simultaneously, the structure of CIPS (1.1 × AGS) is comparable with that of $Rb_2Ga_2P_2S_9$ (0.1 × AGS), which also contains $[P_2S_7]^{4-}$ dimers, thus it can be used to better comprehend the role of geometry distortion of $[InS_6]^{9-}$ and $[P_2S_7]^{4-}$ dimers to improve NLO properties. Herein, it is observed that the basic unit of $Rb_2Ga_2P_2S_9$ is a derivative adamantane-like $[Ga_2P_2S_{10}]^{4-}$ cluster, which is the combination of two $[GaS_4]^{5-}$ tetrahedron and $[P_2S_7]^{4-}$ dimer (Fig. S7 in Supporting information). It is found that $[P_2S_7]^{4-}$ dimers

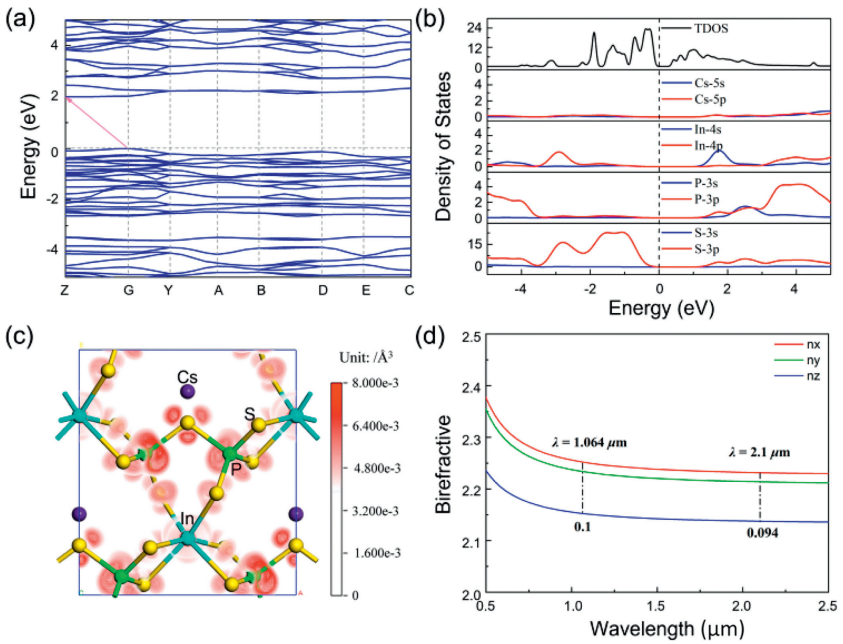

Fig. 4. Theoretical calculation results for CIPS. (a) Band structure. (b) The TDOS and PDOS of CIPS. (c) SHG-density maps of CIPS. (d) Calculated birefringence curve.

adopt a highly twisted conformation in the CIPS (29.347°) due to the increase in coordination of In^{3+} inducing the torsion of $[PS_4]^{3-}$ unit (Fig. S8 in Supporting information). The large calculated dipole moments of $[InS_6]^{9-}$ octahedra and $[PS_4]^{3-}$ tetrahedral in CIPS also prove the strong geometry distortion (Table S6 in Supporting information). Combination of theoretical calculations and structure analysis shows that the coupling of strong distortion $[InS_6]^{9-}$ octahedron and highly twisted $[P_2S_7]^{4-}$ dimers in CIPS significantly contributes to SHG response. It is similar with the situation that the more distorted $[P_2O_7]^{4-}$ dimers in the high-temperature phase of $RbNaMgP_2O_7$ exhibit larger SHG response than that in the low-temperature phase [40].

In summary, CIPS was obtained through high-temperature solid-state method. CIPS is a potential NLO material with balanced performance in the MIR region, which is well verified by the experimental results, including a strong phase-matchable SHG response of 1.1 × AGS, and large laser-induced damage threshold of 20.8 × AGS. Structural analysis and theoretical calculations results show that the coupling of $[InS_6]^{9-}$ octahedra and $[P_2S_7]^{4-}$ dimers make a synergistic contribution to the superior NLO performance. Alkali-metal ion Cs^+ enlarge the band gap and the interaction between $[InS_6]^{9-}$ and $[P_2S_7]^{4-}$ reduce the TEA, which leads to the large LIDTs. This study coupled multiple strategies and design a potential high-performance thiophosphates CIPS, which provide new means for the design of NLO-LIDT compatible materials.

Declaration of competing interest

The authors declare that they have no known competing financial interests or personal relationships that could have appeared to influence the work reported in this paper.

Acknowledgment

This work was financially supported by the Natural Science Foundation of China (No. 22105218).

Supplementary materials

Supplementary material associated with this article can be found, in the online version, at doi:10.1016/j.cclet.2023.109108.

References

[1] D. Richter, A. Fried, B. Wert, et al., Appl. Phys. B 75 (2002) 281–288.
[2] V.A. Serebryakov, É.V. Boĭko, N.N. Petrishchev, A.V. Yan, J. Opt. Technol. 77 (2010) 6–17.
[3] H. Chen, W. Wei, H. Lin, X. Wu, Coord. Chem. Rev. 448 (2021) 214154.
[4] A. Harasaki, K. Kato, Jpn. J. Appl. Phys. 36 (1997) 700–703.
[5] G.C. Catella, L.R. Shiozawa, J.R. Hietanen, et al., Appl. Opt. 32 (1993) 3948–3951.
[6] G.D. Boyd, E. Buehler, F.G. Storz, Appl. Phys. Lett. 18 (1971) 301–304.
[7] J. Cai, Y. Lan, H. He, et al., Inorg. Chem. 59 (2020) 16936–16943.
[8] W. Wang, B. Ji, W. Yao, et al., Sci. China Mater. 64 (2021) 1047–1057.
[9] J. Zhao, D. Mei, Y. Yang, et al., Inorg. Chem. 58 (2019) 15029–15033.
[10] G.Y. Davydyuk, G.L. Myronchuk, G. Lakshminarayana, et al., J. Phys. Chem. Solids 73 (2012) 439–443.
[11] H. Chen, M. Ran, S. Zhou, et al., Chin. Chem. Lett. 34 (2023) 107838.
[12] D. Mei, W. Yin, Z. Lin, et al., Inorg. Chem. 51 (2012) 1035–1040.
[13] W. Xing, F. Liang, C. Tang, et al., ACS Appl. Mater. Int. 13 (2021) 37331–37338.
[14] X. Li, L. Kang, C. Li, et al., J. Mater. Chem. C 3 (2015) 3060–3067.
[15] S. Li, X. Jiang, B. Liu, et al., Chem. Mater. 29 (2017) 1796–1804.
[16] M. Zhang, B. Liu, X. Jiang, G. Guo, Inorg. Chem. Front. 10 (2023) 1112–1118.
[17] B. Liu, H. Zeng, X. Jiang, et al., Chem. Sci. 7 (2016) 6273–6277.
[18] Y. Song, S. Cui, Z. Qian, et al., Inorg. Chem. Front. 9 (2022) 5932–5940.
[19] W. Wang, D. Mei, S. Wen, J. Wang, Y. Wu, Chin. Chem. Lett. 33 (2022) 2301–2315.
[20] M. Li, L. Jiang, S. Pei, et al., J. Mater. Chem. C 10 (2022) 9146–9151.
[21] X. Huang, S. Yang, X. Li, W. Liu, S. Guo, Angew. Chem. Int. Ed. 61 (2022) e202206791.
[22] J. Feng, C. Hu, X. Xu, et al., Chem. Eur. J. 23 (2017) 10978–10982.
[23] V. Maisonneuve, M. Evain, C. Payen, et al., J. Alloys Compd. 218 (1995) 157–164.
[24] Z. Shi, M. Yang, W. Yao, W. Liu, S. Guo, Inorg. Chem. 60 (2021) 14390–14398.
[25] Z. Li, X. Jiang, M. Zhou, et al., Inorg. Chem. 57 (2018) 10503–10506.
[26] A. Gutzmann, C. Näther, W. Bensch, Acta Crystallogr. Sect. E: Struct. Rep. Online 61 (2005) i6–i8.
[27] S.K. Kurtz, T.T. Perry, J. Appl. Phys. 39 (1968) 3798–3813.
[28] M. Zhou, L. Kang, J. Yao, et al., Inorg. Chem. 55 (2016) 3724–3726.
[29] X. Li, Z. Shi, M. Yang, W. Liu, S. Guo, Angew. Chem. Int. Ed. 61 (2022) e202115871.
[30] Y. Han, C. Hu, Z. Fang, et al., J. Mater. Chem. C 10 (2022) 12556–12559.
[31] Q. Hu, K. Ruan, Y. Wang, K. Ding, Y. Xu, New J. Chem. 43 (2019) 12468–12474.
[32] M. Li, Z. Ma, B. Li, et al., Chem. Mater. 32 (2020) 4331–4339.
[33] Z. Li, S. Zhang, Z. Huang, et al., Chem. Mater. 32 (2020) 3288–3296.
[34] I. Bodnar, N. Orlova, Phys. Status Solid A 91 (1985) 503–507.
[35] S. Guo, Y. Chi, H. Xue, Angew. Chem. Int. Ed. 57 (2018) 11540–11543.
[36] S. Guo, X. Cheng, Z. Sun, et al., Angew. Chem. Int. Ed. 58 (2019) 8087–8091.
[37] S. Li, X. Jiang, Y. Fan, et al., Chem. Sci. 9 (2018) 5700–5708.
[38] S. Li, X. Jiang, B. Liu, et al., Inorg. Chem. 57 (2018) 6783–6786.
[39] X. Jiang, N. Wang, L. Dong, et al., Mater. Horiz. 9 (2022) 2207–2214.
[40] S. Zhao, X. Yang, Y. Yang, et al., J. Am. Chem. Soc. 140 (2018) 1592–1595.